Journal of Biomechanics 53 (2017) 45–55

Contents lists available at ScienceDirect

Journal of Biomechanics

journal homepage: www.elsevier.com/locate/jbiomech
www.JBiomech.com

Feasibility of using MRIs to create subject-specific parallel-mechanism joint models

Simao Brito da Luz [a,*], Luca Modenese [a,b,c], Nicola Sancisi [d], Peter M. Mills [a], Ben Kennedy [a], Belinda R. Beck [a], David G. Lloyd [a]

[a] Menzies Health Institute Queensland, Griffith University, Australia
[b] Department of Mechanical Engineering, University of Sheffield, UK
[c] INSIGNEO institute for in silico medicine, University of Sheffield, UK
[d] Department of Industrial Engineering, Health Sciences and Technologies ICIR, University of Bologna, Italy

ARTICLE INFO

Article history:
Accepted 19 December 2016

Keywords:
MRI
Subject-specific
Joint kinematic models
Computer simulation
Modelling

ABSTRACT

Musculoskeletal models typically use generic 2D models for the tibiofemoral (TFJ) and patellofemoral (PFJ) joints, with a hinge talocrural joint (TCJ), which are scaled to each subject's bone dimensions. Alternatively joints' measured kinematics in cadavers are well-predicted using 3D cadaver-specific models. These employ mechanisms constrained by the articulations of geometric objects fitted to the joint's surfaces.

In this study, we developed TFJ, PFJ and TCJ mechanism-based models off MRIs for fourteen participants and compared the estimated kinematics with those from published studies modified to be consistent with mechanisms models and subject-specific anatomical landmarks. The models' parameters were estimated by fitting spheres to segmented articular cartilage surfaces, while ligament attachment points were selected from their bony attachment regions.

Each participant's kinematics were estimated by ensuring no length changes in ligaments and constant distances between spheres' centres. Two parameters' optimizations were performed; both avoid singularities and one best matches the kinematic patterns off published studies. Sensitivity analysis determined which parameters the models were sensitive to.

With both optimization methods, kinematics did not present singularities but correlation values were higher, exceeding 0.6, when matching the published studies. However, ranges of motion (ROM) were different between estimated and published studies. Across participants, models presented large parameter variation. Small variations were found between estimated- and optimized-parameters, and in the estimated-rotations and translations' means and ROM. Model results were sensitive to changes in distal tibia, talus and patella spheres' centres. These models can be implemented in subject-specific rigid-body musculoskeletal models to estimate joint moments and loads.

1. Introduction

Musculoskeletal models are important tools to understand human motion. However most models in software such as Anybody (Damsgaard et al., 2006) or OpenSim (Delp et al., 2007) are generic (Arnold et al., 2010; Delp et al., 1990; Modenese et al., 2011). These models' bone sizes and joint kinematics were derived from a limited number of cadavers, which are then scaled to each subject using motion capture markers placed on the skin. However, scaling is error-prone since it relies on the examiners' skill to palpate bony landmarks (Della Croce et al., 1999). Furthermore, these models represent the tibiofemoral (TFJ) and patellofemoral (PFJ) joints using simple two-dimensional (2D) planar mechanisms (Walker et al., 1988; Yamaguchi and Zajac, 1989) or the talocrural joint (TCJ) as a hinge (Isman and Inman, 1968). These generic models may be adequate for certain research questions (Hicks et al., 2015), but may not estimate three-dimensional (3D) joint kinematics. Importantly, compared to subject-specific musculoskeletal models derived from medical imaging, scaled-generic models have worse predictions of measured joint contact forces (Gerus et al., 2013; Lerner et al., 2015), moments (Tsai et al., 2012) and angles (Scheys et al., 2011). Therefore, models that incorporate subject-specific skeletal-joint anatomy are needed.

Subject-specific joint kinematics can be measured *in vivo* using fluoroscopy (Lu et al., 2008) or biplanar radiography (Clément et al.,

* Correspondence to: Griffith University, Gold Coast Campus, Parklands drive, 4222 Queensland, Australia.
E-mail address: simao.britodaluz@griffithuni.edu.au (S. Brito da Luz).

http://dx.doi.org/10.1016/j.jbiomech.2016.12.018
0021-9290/

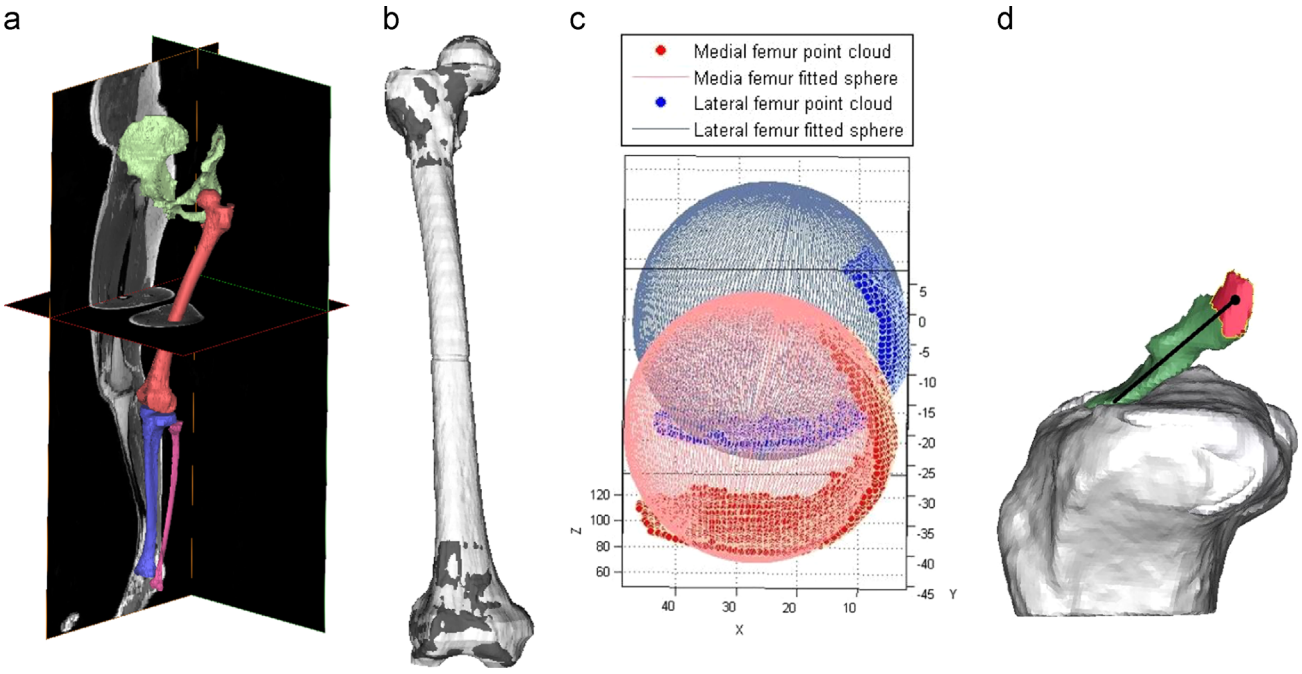

Fig. 1. Procedure to generate subject-specific joint model parameters from MRI: a) Bone segmentation from MRIs, b) alignment (registration) of 3D femoral surfaces from bone and joint scans, c) example of sphere fitting to articular surfaces, in this case the femoral condyles, and d) example of 3D ligament surface, in this case the ACL, with femoral attachment surface (in red), surface centroid (point) and ligament link (line) are shown. (For interpretation of the references to colour in this figure legend, the reader is referred to the web version of this article.)

2015). However their availability, radiation exposure, lengthy imaging procedures and/or high costs limit their application. Alternatively, rigid-body-mechanism-based models with geometric objects representing joint tissues can be employed, which have successfully predicted measured TFJ, PFJ, and TCJ passive kinematics in cadavers (Franci et al., 2009; Sancisi and Parenti-Castelli, 2011). These models, including isometric ligaments, estimate all rotations and translations, but to-date have only been included in generic models (Duprey et al., 2010).

Mechanism-based joint models could potentially estimate *in vivo* joint 3D-kinematics, with MRI-derived parameters from each individual's, but this is yet to be done. However, these mechanisms are highly sensitive to parameter variations (Sancisi et al., 2011), so MRI-derived parameters may have to be optimized to avoid kinematic singularities and non-physiological motion. The aforementioned cadaveric models were optimized by matching the estimated kinematics with those measured from the same cadaver, but *in vivo* measured kinematics are generally not available. However, published kinematics could be used as a reference, although these are generally representative of a wide range of subjects and are expressed in disparate CFs; therefore, these kinematics could perhaps be made more subject-specific if their CFs are transformed to be consistent with the mechanisms model and a small set of subject-specific parameters that are extracted from MR images at a single joint angle. So a robust method to create MRI-derived subject-specific optimized mechanisms is required. Previous subject-specific rigid-body models (Kainz et al., 2016; Sreenivasa et al., 2016; Valente et al., 2015) used various MRI-derived joint models e.g. 4-bar mechanism, hinges and spherical respectively; however, these models cannot estimate all 3D-kinematics.

This study presents new methods to create subject-specific TFJ, PFJ and TCJ rigid-body mechanism-based models from *in vivo* MRIs. Two optimization algorithms were developed: Optim1) avoids singularities, and Optim2) avoids singularities and tracks the published studies' kinematic curves patterns. Furthermore, a method was developed to transform published kinematics. We hypothesized that: (i) both optimized models' kinematics will be subject-specific with no singularities, but Optim2 will also estimate physiologically-believable motion since it will well-correlate with the published kinematics' curves patterns, but with potential differences in the ROMs and curve offsets, (ii) estimated- and optimized-parameters will be similar, (iii) estimated- and optimized-parameters will vary across participants, (iv) means and ROM of the estimated kinematics' will be different across participants, and (v) differences in joint geometry i.e. tibia plateaus' concavity depth, between two participants will lead to kinematic differences. Finally we established how sensitive the models were to the optimized-parameters.

2. Methods

2.1. MRI acquisition and processing

Griffith University Human Research Ethics Committee (PES/37/11/HREC) approved all procedures. Fourteen healthy participants provided their informed, written consent and had no history of relevant musculoskeletal abnormalities: 12 M and 2 F, 30 ± 5.7y, 1.8 ± 0.08 m (1.62m-1.91 m), 77 ± 13 kg (53 kg-93 kg), with 23.8 ± 3.06 kg/m^2 BMI. Bone and joint scans were acquired from nine left and five right limbs using a Philips Ingenia 3 T MRI machine (Netherlands). MRI sequences were set to optimize the visibility of bone-cartilages and ligaments, with short scan times. All lower limb bones were imaged, superior to the iliac crest to the plantar foot surfaces, using axial 2D T1W with 1mm gap between slices, and $0.59 \times 0.59 \times 5$ mm reconstructed voxels. 3D sagittal plane hip, knee and ankle joint scans had no gap and small slice thicknesses to discriminate the different joint tissues, with the following sequence, reconstructed voxel size: (i) hip: T1W fat-sat 3D FFE Dixon, $0.29 \times 0.29 \times 1.5$ mm reconstruction, (ii) knee and ankle: T1W 3D FFE, $0.29 \times 0.29 \times 1$ mm reconstruction. The knee and ankle joint scans were acquired in the MRI reference pose (Appendix B), which across participants was $14.0 \pm 5.6°$ of knee flexion and $4.7 \pm 3.3°$ of ankle flexion.

The 3D anatomical surfaces were created by segmenting the bones, cartilage and ligaments in each MRI slice (Fig. 1a) using Mimics (Materialise, Leuven). The bone and cartilage surfaces included the pelvis, femur, tibia, fibula, patella, talus and calcaneus. Ligaments included the anterior cruciate (ACL), posterior cruciate (PCL), medial collateral (MCL) for the TFJ, patella tendon (PT) for the PFJ and

calcaneofibular (CaFi) and tibiocalcaneal (TiCa) for the TCJ, the main ligaments guiding each of these joints' motion (Leardini et al., 1999; Wilson et al., 1998). The Mimics iterative closest point alignment algorithm was used to assemble complete bones, with their associated cartilage and ligaments, by registering the bone surfaces to the equivalent bone surfaces on the joint scans (Fig. 1b). For each participant, MRI segmentation and 3D surfaces' construction were completed in ~11 h.

2.2. Joint mechanism formulations

All joints were modelled as mechanisms incorporating articulating spheres constrained by rigid ligaments (Franci et al., 2009; Sancisi and Parenti-Castelli, 2011) (Appendices A and B). For the TFJ and TCJ the ligament fibres were assumed to be isometric (Fuss, 1989; Leardini et al., 1999; Rovick et al., 1991), while constant distances were maintained between the centres of spheres fitted to the articular cartilage surfaces, i.e. these fitted spheres "rolled and slid" without penetration or lift-off. For the PFJ, the patella body moved at a fixed distance around a skewed hinge axis, defined by the centres of spheres fitted to medial and lateral femoral patellar surfaces, while maintaining constant PT length. All mechanism links lengths were constant when solving each joint model's equations (Appendix A).

The CFs used in the joint mechanisms, now called mechanism-CFs, followed previous definitions (Appendix B, Table B.1): the femur and patella CFs as per Belvedere et al. (2007) and talus as in Sancisi et al. (2014). Two tibial CFs were defined; one proximal for the TFJ and PFJ (Belvedere et al., 2007), and one distal for the TCJ model (Sancisi et al., 2014). For the TFJ and PFJ the tibia and patella motion was expressed relative to the femur, while the talus motion was relative to the tibia in the TCJ.

Each joint's modelled kinematics were estimated as a function of a single independent degree of freedom (DoF). TFJ flexion angle (between 0° and 90°) was the DoF for the TFJ and PFJ, while the TCJ used TCJ dorsiflexion angle (between −25° and 15°). The estimated joint kinematics entailed abduction-adduction (AA) and internal-external (IE) rotations and the anterior-posterior (AP), proximal-distal (PD) and medial-lateral (ML) translations. PFJ model also estimated the PFJ flexion-extension (FE) rotation. All rotations and translations were consistent with the ISB recommended orders of rotation, i.e. ZXY (Grood and Suntay, 1983; Wu et al., 2002). FE was the first rotation about fixed *Z*-axis of the "parent" frame, the second, AA about floating *X*-axis and the third, IE about fixed *Y*-axis of the "child" frame, with flexion, adduction and internal rotation being positive. For the TCJ, the IE was about the *X*-axis and the AA about the *Y*-axis. Anterior, proximal and lateral translations, or *x*, *y* and *z* respectively, were considered positive.

2.3. Geometrical parameters

The models' parameters were obtained by fitting spheres and rigid links to the joints' surfaces in the MRI-reference pose, and expressed in their respective bone CFs (Appendix A, B). Spheres were fitted to the bone and cartilage surfaces using Matlab (R2012a, MathWorks) (Fig. 1c). The fitted surfaces comprised the: (i) medial and lateral femoral condyles (${}^{FEM}B_4$, ${}^{FEM}B_5$) and tibial plateau (${}^{TIB}A_4$, ${}^{TIB}A_5$) for TFJ, (ii) distal-medial fibula (${}^{TIB}F_3$) and lateral talus (${}^{TAL}E_3$) on the talofibular articulation, and medial and lateral aspects of the tibial mortise ${}^{TIB}F_4$, ${}^{TIB}F_5$) and trochlea tali (${}^{TAL}E_4$,${}^{TAL}E_5$) for TCJ, (3) medial and lateral femoral patellar for PFJ (${}^{FEM}p_1$,${}^{FEM}p_2$). The spheres' parameters included the centre coordinates and distances between articulating sphere centres.

The intersection of each segmented ligament with the bones' surfaces defined the ligament-attachment regions. These regions' centroids represented the ligament attachment points (Fig. 1d): 1) TFJ; ACL, PCL and MCL (respectively $i = 1, 2, 3$) in the femur (${}^{TIB}A_i$)and tibia (${}^{FEM}B_i$), 2) PFJ; patella tendon in the tibia (${}^{TIB}C$) and patella (${}^{PAT}D$), and 3) TCJ; CaFi and TiCa (respectively $i = 1, 2$) in the calcaneus (${}^{TAL}E_i$), fibula and tibia (${}^{TIB}F_i$). The Euclidean distances between centroids defined each ligament's linkage length. Specific PFJ models' parameters were also defined (Appendix A and B).

2.4. Parameter optimization

Each participant's estimated-parameters were optimized to ensure that their corresponding joint mechanisms could be solved. Two optimizations' algorithms (Optim1 and Optim2) were developed: both avoided mechanism singularities while Optim2 also ensured the estimated kinematic patterns were similar to published kinematics. Both optimizations had inner and outer loops. The inner used Matlab's "*fsolve*" function to solve each mechanism's system of equations for 1° increments of the independent DoF. Using Matlab's simulated annealing function, the outer loop optimized model parameters to minimize one of two objective functions:

$$\begin{aligned} G_1 &= w_1 f_1 + w_2 f_2 \; for \; Optim1, \; or \\ G_2 &= w_1 f_1 + w_2 f_2 + w_3 f_3 \; for \; Optim2 \end{aligned} \quad (1)$$

where f_1, f_2, and f_3 are different optimization criteria and w_1, w_2, and w_3 are the respective weightings.

Criteria f_1 included two processes to avoid mechanism singularities and ensure continuous kinematics. Singularities occurred when the mechanisms equations could not be solved at any flexion angle. If this occurred, the inner loop terminated and f_1 value was set to 1000. Without singularities, the second process ensured continuous kinematics across the DoF's full ROM. After experimenting with different methods, a 3rd order polynomial was fitted to each kinematic curve, and a RMS difference (RMSD) was calculated between the kinematics and respective polynomial. $f_1$had the largest RMSD from each joint.

Criteria f_2 ensured the optimized-parameters were close to the estimated values, thereby well representing the modelled anatomical elements. Thus, f_2 was the RMSD between the estimated- and optimized-parameters.

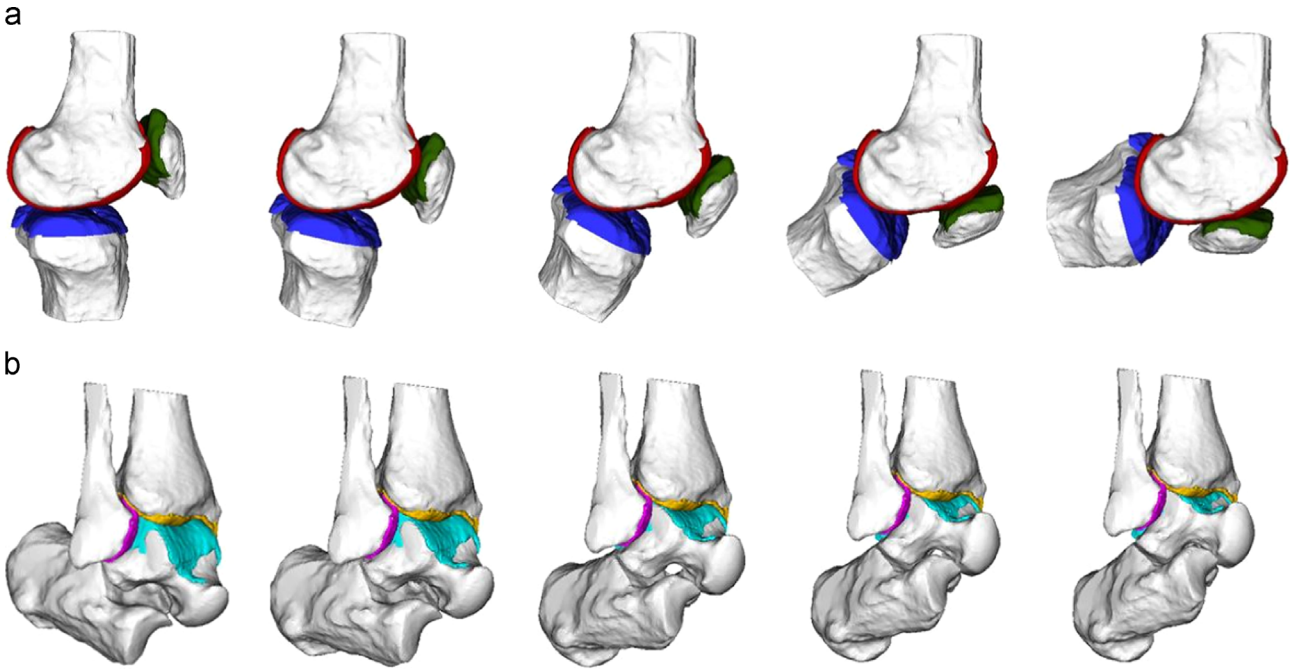

Fig. 2. Visualization of one participant's subject-specific 3D surfaces from the MRIs articulating with kinematic results from the joint models: a) TFJ and PFJ model results for TFJ flexion angle between 0° and 90°, and b) TCJ model results for TCJ dorsiflexion angle between −25° and 15°.

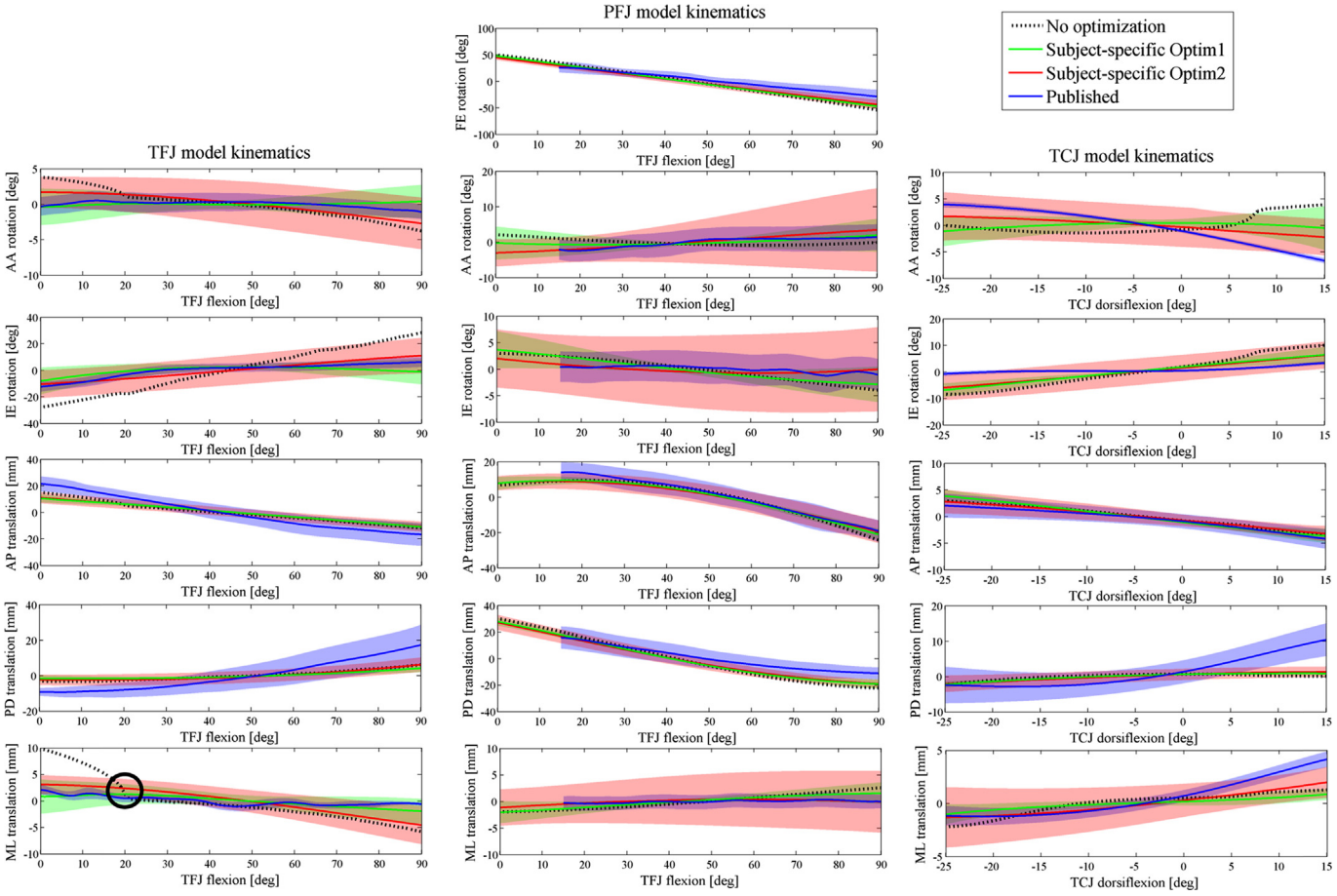

Fig. 3. Subject-specific TFJ (left), PFJ (middle) and TCJ (right) model kinematic outputs from non-optimized model ($n=1$), Optim1 (average $\pm$ std in red), Optim2 (average $\pm$ std in green) and from published studies (average $\pm$ std in blue). Published studies included: (1) for the TFJ model; Ottoboni et al., (2010) and Sancisi and Parenti-Castelli (2011), (2) PFJ model; Anglin et al. (2008) and Sancisi and Parenti-Castelli (2011) and (3) TCJ model; Franci et al. (2009) and Sancisi et al. (2014). FE (flexion-extension), AA (abduction-adduction), IE (internal-external) rotations and AP (anterior-posterior), MD (medial-lateral), PD (proximal-distal) translations are plotted versus the flexion angle of the tibia (TFJ and PFJ models) and talus (TCJ model). The mean of each kinematic curve was subtracted from the curve to facilitate visual inspection and because some published kinematics only reported offset kinematics. In the non-optimized curves, singularities can be observed for the TFJ ($\sim 21^\circ$ of TFJ flexion as highlighted) and TCJ ($\sim 7^\circ$ of TCJ flexion). (For interpretation of the references to colour in this figure legend, the reader is referred to the web version of this article.)

Criteria f_3 maximized the Pearson's correlation, ρ_i, between the estimated and transformed published kinematics (Appendix C, Fig. C.1), i.e.

$$f_3 = \begin{array}{l} minmax(1-\rho_i)^2 (i=1,\ldots,5)\, for\ TFJ, TCJ\ models \\ (i=1,\ldots,6)\, for\ PFJ\ model \end{array} \quad (2)$$

Minmax was used to maximize the lowest ρ_i and ensured high correlations for all joint's kinematics. The published data comprised of 6 sets of published passive kinematics measured *in vitro* from cadavers or *in vivo* from healthy participants. The cadaveric studies included: TFJ; Ottoboni et al. (2010) and Sancisi and Parenti-Castelli (2011), PFJ; Sancisi and Parenti-Castelli (2011) and TCJ; Franci et al. (2009) and Sancisi et al. (2014). *In vivo* studies comprised of Anglin et al. (2008) for the PFJ.

All joints' published kinematics were expressed in a range of disparate published-CFs. Therefore, to be expressed in the mechanism-CFs, the published kinematics were transformed to each participant. The published studies only named the anatomical landmarks used to create their published-CFs without providing their actual numerical 3D locations. Subsequently, the corresponding anatomical landmarks were located on each participant's bone meshes from which participant-equivalent published-CFs were created. Transformation matrices from the participant-equivalent published-CFs to mechanism-CFs were then determined, e.g. for the TFJ, T_1 represents the transformation of the femur's participant-equivalent published-CFs to the mechanism-CFs and similarly T_3 is the transformation for the tibial CFs. For each study's published kinematics, T_2 was defined as the transformation between the two articulating bones, e.g. tibia relative to the femur, from which we determined the transformed published kinematics, T_f, for each participant, i.e.

$$T_f = T_1 * T_2 * T_3 \quad (3)$$

henceforth just called published kinematics. Since some studies offset the kinematics to vary around zero, the mean of each transformed kinematic curve was subtracted to create "zeroed" curves. Then, ensemble-average curves were created for the zeroed TFJ and PFJ published kinematics, while a 5th order polynomial was fitted to the "zeroed" TCJ transformed kinematics, because these data sets' kinematics were across multiple different ranges of TCJ dorsiflexion (see supplementary data).

The weights w_1 and w_2 (Eq. (1)) were selected so that f_1 and f_2 values had orders of magnitude of 10°. However, w_3 was set so f_3 had an order of magnitude 10^1, which ensured Optim2's kinematics well matched the published kinematics, to contrast with Optim1 method.

G_1 and G_2 were minimized by optimizing various model parameters. These comprised of the ligaments' attachments and spheres' centres locations, except for the femoral condyles since these were well fitted with small residuals values (0.8 ± 0.19 mm). The optimized ligament attachment points were kept within their bone attachment regions. All constant ligament lengths, sphere radii, and PFJ model parameters were updated for the MRI-reference pose using the optimized ligament attachment points and sphere centres. The radius of each optimized sphere was updated by minimizing the summed least squares residuals between each sphere and MRI cartilage 3D surface. However, the modified spheres' centres were constrained to ensure the sphere's least squares residuals were less than 5% of the optimized radius. Both optimizations required $\sim$10 h using a 3.4 GHz-Intel i7-2600 with 16 GB-RAM.

2.5. Analyses

Five analyses, corresponding to hypotheses, and a sensitivity analysis were undertaken with associated statistical tests using a $p < 0.05$ and Benjamini and Hochberg (1995) p-value corrections for multiple comparisons. *Analysis-1* examined the similarity of Optim1 and Optim2 kinematic curves' patterns with those from published kinematics using Pearson's correlations (ρ). The difference between the Optim1 and Optim2 ρ's was tested using a Wilcoxon rank test.

Preempting the results, compared to Optim1, Optim2's estimated kinematics were more similar to the published kinematics. Therefore, all remaining five analyses used

Optim2. *Analysis-2* used paired t-tests to compare estimated and published kinematics' ROMs over the published studies' FE excursions, i.e. PFJ was between 15° to 90°. This analysis also assessed the differences between estimated- and optimized-parameter and spheres' residuals using paired t-tests and RMSD. *Analysis-3* examined participant differences in the estimated- and optimized-parameters using their standard deviations (STD) relative to their average. *Analysis-4* examined the differences in the estimated kinematics' means and ROMs across participants, using their STD's relative to their averages as percentages. Estimated TFJ and PFJ means and ROMs were calculated for FE from 0° to 90°, while TCJ from −25° to 15°. *Analysis-5* compared the effects of joint geometry on the TFJ model kinematics from two participants with very different tibial plateau' sphere sizes.

In the sensitivity analysis each optimized-parameter's *x, y, z* coordinates were varied individually and G_2 recalculated. Coordinates were incremented by δ until μ deviation from the optimized-parameter value was reached. δ and μ were respectively ±0.1 mm and ±10 mm for the TFJ and PFJ sphere centres, and ±0.05 mm and ±5 mm for all ligament attachments and TCJ spheres' centres. A quadratic polynomial was fitted to each incremented-parameter coordinate and corresponding G_2's in the region around the minimum G_2. Subsequently, higher quadratic coefficients indicated models more sensitive to a particular coordinate.

3. Results

Geometric objects were fitted to the MRIs to create personalized joints (e.g. Fig. 2). However, before parameter optimization, all participants' TFJ and TCJ models had singularities (e.g. Fig. 3), while after Optim1 and Optim2, all kinematics were continuous and without singularities. Transformed published joint kinematics were created (App. C, supplementary materials), which enabled Optim2 optimization and the analysis of the models estimated kinematics.

In *Analysis-1,* Optim2 kinematics had significantly higher correlations with the published kinematics compared to Optim1 (Fig. 3, Table 1). This was for all the joints' AA and ML, TFJ IE and TCJ PD ($p \leq 0.05$). Optim2 kinematics exhibited high correlations ($\rho \geq 0.7$, $p < 0.03$), except for the PFJ IE ($\rho = 0.6$, $p < 0.04$), and the TCJ ML had non-significant correlation.

In *Analysis-2,* the estimated and published kinematics' ROMs were different for all joints ($p < 0.03$) (Table 2), except for the TFJ IE, PFJ AA and TCJ IE and ML.

Analysis-2 also revealed that estimated- and optimized-parameters were generally similar, although some parameters had significant but small differences (Tables 3–5). Optimized-fitted-sphere residuals (0.88 ± 0.3 mm) were mostly significantly higher than the initial residuals (0.46 ± 0.14 mm) ($p \leq 0.03$). Additionally, the RMSD between the estimated- and optimized-parameters for all models (Tables 3–5) varied between 0.31 ± 0.21 mm and 12.2 ± 8.8 mm. Furthermore, the RMSD for the TFJ ligaments' insertions and sphere centres were between 1.04 ± 0.76 mm and 12.2 ± 8.8 mm, with an average value of 4.3 mm.

In *Analysis-3,* the coordinates of the spheres' centres had generally larger variations across participants, with higher STDs, when compared with the ligaments' attachment points (Tables 3–5). The higher STDs were found for the *y* coordinates of the TFJ spheres' centres and for the TCJ ${}^{TIB}F_3$,${}^{TAL}E_3$ spheres' centres (≥194%). However, the PFJ spheres' centres *x* and *z* coordinates had relatively small STDs (<42%).

In *Analysis-4* we observed large variations, with high STDs, in the means and ROMs of the estimated rotations' across participants (Table 2). Higher STDs were found for the TFJ and AA's and PFJ IE's mean (688% and 145%). Comparatively, the estimated translations' means and ROMs exhibited lower variations, although the TFJ ML's mean as well as the TCJ AP's mean showed large STDs (7081% and 110%).

Analysis-5's selected participants had large differences in the TFJ lateral tibial spheres' centres, but smaller differences for medial tibial spheres' centres (Fig. 4). Furthermore, their TFJ

Table 1
Pearson's correlation coefficients across participants (average ± std) between TFJ, PFJ and TCJ published and Optim1 and Optim2 estimated kinematics.

Joint	Optimization	Rotations			Translations		
		FE	AA	IE	AP	PD	ML
TFJ	Optim1	–	§0.06 ± 0.66	§0.29 ± 0.74	0.98 ± 0.01	0.89 ± 0.20	§0.19 ± 0.76
	Optim2	–	0.80 ± 0.11	0.89 ± 0.05	0.99 ± 0.01	0.96 ± 0.05	0.79 ± 0.09
PFJ	Optim1	1.00 ± 0.00	§-0.06 ± 0.88	0.29 ± 0.63	0.99 ± 0.01	1.00 ± 0.00	§0.22 ± 0.74
	Optim2	1.00 ± 0.00	0.67 ± 0.52	0.60 ± 0.41	0.99 ± 0.01	1.00 ± 0.00	0.76 ± 0.29
TCJ	Optim1	–	§-0.32 ± 0.80	0.87 ± 0.04	0.97 ± 0.02	§0.72 ± 0.12	§0.69 ± 0.46
	Optim2	–	0.83 ± 0.37	0.88 ± 0.04	0.98 ± 0.05	0.85 ± 0.03	0.92 ± 0.08

§ Differences between Pearsons correlation coefficients from Optim1 and Optim2 using a Wilcoxon rank test ($p < 0.05$).

Table 2
Subject-specific kinematic curves' means and ROMs (average ± std) and published curves' ROMs (average ± std). Shown are FE (flexion-extension), AA (abduction-adduction), IE (internal-external) rotations and AP (anterior-posterior), PD (proximal-distal), ML (medial-lateral) translations.

Kinematic metric	Model/measured	Joint	Rotations			Translations		
			FE(deg)	AA(deg)	IE(deg)	AP(mm)	PD(mm)	ML(mm)
Mean	Optim2	TFJ	–	−0.42 ± 2.88	−22.27 ± 10.90	−12.33 ± 3.09	−23.81 ± 3.19	−0.03 ± 2.06
		PFJ	−31.07 ± 5.96	4.68 ± 5.84	-4.31 ± 6.27	40.71 ± 5.03	−13.56 ± 3.92	6.29 ± 4.40
		TCJ	–	15.07 ± 3.63	4.18 ± 4.70	1.13 ± 1.25	8.29 ± 1.70	−6.41 ± 1.73
ROM	Optim2	TFJ	–	§4.62 ± 2.42	21.82 ± 8.38	§21.70 ± 5.65	§9.05 ± 3.40	§7.87 ± 3.10
	Published studies	TFJ	–	1.62 ± 0.00	18.61 ± 0.00	38.12 ± 0.00	26.54 ± 0.00	3.15 ± 0.00
	Optim2	PFJ	88.44 ± 8.83	9.53 ± 10.32	6.42 ± 4.88	28.80 ± 4.81	46.17 ± 6.13	4.17 ± 3.18
		PFJ[a]	§72.89 ± 7.39	8.28 ± 9.08	§5.13 ± 3.66	§28.58 ± 4.71	§35.79 ± 5.32	§3.30 ± 2.38
	Published studies	PFJ	54.25 ± 0.55	4.20 ± 1.74	2.42 ± 1.11	33.22 ± 2.58	26.86 ± 2.79	1.53 ± 0.79
	Optim2	TCJ	–	§4.54 ± 2.82	12.25 ± 4.83	§6.08 ± 2.56	§3.37 ± 1.52	3.50 ± 2.77
	Published studies	TCJ	–	14.07 ± 3.86	14.54 ± 3.95	14.58 ± 0.88	15.48 ± 0.90	2.16 ± 0.37

[a] PFJ ROM of subject-specific model was calculated between 15° and 90° of the TFJ FE ROM to match the published studies' data.
§ Difference between Optim2 subject-specific and published ROMs (paired *t*-tests, $p < 0.03$).

Table 3
The TFJ models' locations of the ligaments' attachments, spheres' centres, links' lengths and spheres' radii (average ± std), estimated from the MRIs and adjusted by optimization.

Direction	Estimated/optimized	Locations in the proximal tibia (mm)									
		ACL (${}^{TIB}A_1$)	RMSD	PCL (${}^{TIB}A_2$)	RMSD	MCL (${}^{TIB}A_3$)	RMSD	Medial plateau (${}^{TIB}A_4$)	RMSD	Lateral plateau (${}^{TIB}A_5$)	RMSD
X	Estimated	12.01 ± 2.48	3.09 ± 2.08	−14.90 ± 3.15	1.87 ± 1.53	−2.01 ± 6.19	3.95 ± 3.96	−7.17 ± 197.07	10.87 ± 8.52	14.76 ± 19.83	8.09 ± 7.46
	Optim2	9.89 ± 3.95		−16.15 ± 2.48		−5.17 ± 8.42		−105.99 ± 196.17		18.72 ± 22.68	
Y	Estimated	−2.30 ± 1.17	1.04 ± 0.76	−9.87 ± 2.39	2.45 ± 2.07	§−37.89 ± 8.08	6.30 ± 3.41	411.55 ± 796.67	10.97 ± 4.08	-39.56 ± 203.65	8.35 ± 6.08
	Optim2	−1.90 ± 1.31		−11.04 ± 3.73		−43.07 ± 11.04		410.08 ± 799.32		−38.11 ± 204.75	
Z	Estimated	−7.72 ± 2.22	3.00 ± 2.74	7.45 ± 3.52	2.63 ± 2.23	§−23.26 ± 5.36	3.48 ± 2.27	−85.23 ± 130.05	12.24 ± 8.82	11.23 ± 29.64	10.54 ± 6.60
	Optim2	−5.96 ± 4.22		9.02 ± 5.51		−20.35 ± 6.45		−82.92 ± 138.20		14.77 ± 38.05	
		Locations in the femur (mm)									
		ACL (${}^{FEM}B_1$)	RMSD	PCL (${}^{FEM}B_2$)	RMSD	MCL (${}^{FEM}B_3$)	RMSD	Medial condyle (${}^{FEM}B_4$)	RMSD	Lateral condyle (${}^{FEM}B_5$)	RMSD
X	Estimated	§−14.41 ± 2.87	2.69 ± 2.07	§−6.20 ± 5.32	4.06 ± 3.85	§5.50 ± 3.30	7.58 ± 3.21	−3.22 ± 2.09	–	−2.40 ± 1.78	–
	Optim2	−12.38 ± 2.89		−2.29 ± 3.80		−2.08 ± 2.47		–		–	
Y	Estimated	−1.94 ± 3.40	3.35 ± 2.02	§−10.67 ± 2.44	1.78 ± 1.25	§−2.35 ± 2.43	2.51 ± 1.95	−6.39 ± 2.13	–	−3.21 ± 3.42	–
	Optim2	−1.77 ± 5.17		−9.28 ± 2.06		−4.36 ± 2.39		–		–	
Z	Estimated	§12.49 ± 2.46	2.19 ± 1.88	§−10.36 ± 2.55	3.09 ± 1.87	−41.91 ± 4.74	0.69 ± 0.48	−25.38 ± 2.67	–	27.80 ± 2.88	–
	Optim2	10.49 ± 2.73		−7.27 ± 3.37		−41.69 ± 4.27		–		–	
		Linkage lengths (mm)									
		ACL (${}^{TFJ}L_1$)	RMSD	PCL (${}^{TFJ}L_2$)	RMSD	MCL (${}^{TFJ}L_3$)	RMSD	Medial Spheres (${}^{TFJ}L_4$)	RMSD	Lateral Spheres (${}^{TFJ}L_5$)	RMSD
Lengths	Estimated	§39.38 ± 5.74	3.98 ± 2.88	§30.50 ± 4.21	5.10 ± 3.35	§67.54 ± 8.57	5.55 ± 3.37	431.99 ± 817.43	10.15 ± 4.78	153.22 ± 146.85	8.64 ± 5.55
	Optim2	36.14 ± 6.62		34.96 ± 4.72		69.46 ± 11.24		430.60 ± 820.82		153.52 ± 149.78	

		Radii (mm)							
		Medial femoral condyle (${}^{FEM}r_1$)	RMSD	Lateral femoral condyle (${}^{FEM}r_2$)	RMSD	Medial tibial plateau (${}^{TIB}r_1$)	RMSD	Lateral tibial plateau (${}^{TIB}r_2$)	RMSD
Radii	Estimated	26.08 ± 2.38	–	25.04 ± 2.96	–	453.99 ± 819.10	10.09 ± 4.63	136.70 ± 155.77	8.56 ± 5.16
	Optim2	–		–		452.45 ± 822.57		137.07 ± 158.69	

§ Difference (with paired *t*-tests) between estimated and optimized (from Optim2) values ($p < 0.04$).

Table 4
The PFJ model's locations of spheres' centres, patella tendon (PT) attachments, PT and λ lengths and spheres' radii (average ± std), estimated from the MRI and adjusted by optimization.

Direction	Estimated/optimized	Location of femoral patellar sphere centres (mm)			
		Medial patellar (${}^{FEM}p_1$)	RMSD	Lateral patellar (${}^{FEM}p_2$)	RMSD
X	Estimated	11.79 ± 4.99	2.62 ± 1.90	§13.85 ± 2.79	3.66 ± 1.19
	Optim2	11.88 ± 4.79		10.19 ± 3.15	
Y	Estimated	§0.62 ± 3.49	2.93 ± 1.75	3.83 ± 3.30	2.58 ± 1.78
	Optim2	3.20 ± 3.61		5.38 ± 4.74	
Z	Estimated	−17.17 ± 3.51	2.80 ± 1.38	21.99 ± 2.81	2.78 ± 1.44
	Optim2	−16.50 ± 4.87		22.53 ± 3.61	
		Location of PT in tibia and patella (mm)			
		PT(${}^{TIB}C$)	RMSD	PT(${}^{PAT}D$)	RMSD
X	Estimated	36.70 ± 4.76	1.77 ± 1.92	4.96 ± 2.62	1.32 ± 0.88
	Optim2	36.72 ± 5.59		5.77 ± 2.97	
Y	Estimated	−30.60 ± 5.31	4.86 ± 5.49	§−19.22 ± 2.95	2.35 ± 1.99
	Optim2	−33.27 ± 8.50		−17.47 ± 3.66	
Z	Estimated	§−10.56 ± 5.97	6.01 ± 3.73	§3.40 ± 2.58	6.15 ± 5.03
	Optim2	−6.34 ± 7.78		−1.57 ± 5.70	
		Links lengths (mm)			
		PT(${}^{PFJ}L$)	RMSD	λ	RMSD
Length	Estimated	§58.08 ± 9.81	8.00 ± 6.65	3.43 ± 1.90	0.31 ± 0.21
	Optim2	65.29 ± 11.23		3.38 ± 2.02	
		Radii of the femoral patellar spheres (mm)			
		Medial patellar (${}^{FEM}r_3$)	RMSD	Lateral patellar (${}^{FEM}r_4$)	RMSD
Radii	Estimated	28.76 ± 5.46	2.99 ± 1.70	§29.92 ± 2.95	3.80 ± 1.88
	Optim2	30.64 ± 5.79		33.51 ± 3.64	

§ Difference between estimated and Optim2 optimized values (paired t-tests, $p < 0.05$).

kinematics presented similar curves' patterns, but different ROMs: (i) all kinematics were highly correlated ($\rho \geq 0.7$, $p \leq 0.05$) and (ii) participants' 1 AP's ROM was 6.3 mm lower, PD's ROM was 7.8 mm higher and AA's ROM was 8° higher than participants' 2 (Fig. 4).

The sensitivity analysis showed the models were sensitive (Table 6, Supplement materials) to the TCJ ${}^{TIB}F_4$, ${}^{TIB}F_5$, ${}^{TAL}E_4$, ${}^{TAL}E_5$ as well as the x and y coordinates of the PFJ spheres' centres had the highest quadratic coefficients (≥ 0.17), while the PFJ patella tendon and TFJ ${}^{TIB}A_2$, ${}^{TIB}A_3$ ligaments' attachment points had the smallest coefficients (≤ 0.01), with the rest between these extremes.

4. Discussion

For the first time, subject-specific TFJ, PFJ and TCJ mechanisms' models were created for fourteen participants from their MRIs. Mechanisms have been previously used to estimate *in vivo* joint angles, but only assembled and used as a generic model (Duprey et al., 2010). Without optimization, all participants' TFJ and TCJ mechanisms produced singularities, which was previously reported, since these mechanisms are highly sensitive to parameters' variation (Sancisi et al., 2011). Therefore, parameters from MRIs need to be optimized to avoid singularities. After both optimizations, all estimated kinematics were without singularities.

Optim1 estimated kinematics generally exhibited smaller and some negative correlations to published kinematics compared to Optim2, supporting hypothesis 1. Understandably, Optim2 estimated kinematics were similar to published kinematics, since the tracking kinematic patterns was an optimization criteria. The moderate correlations for Optim2 PFJ IE rotations were probably due to their small ROMs. Optim2 basically estimates the subject-specific kinematics by tracking the published kinematics, but forcing the model to respect the participant's anatomical constraints. This is important for future implementations, since Optim2 can be used to ensure physiological representative motion without using the individuals measured kinematics, which is not usually available and was required on the previous cadaveric joint models (Franci et al., 2009; Sancisi and Parenti-Castelli, 2011).

Despite having similar patterns, the estimated- and published-kinematic ROMs were generally different, particularly for the TFJ and TCJ, supporting hypothesis 2. These differences may be due to different joint geometries across individuals. However, optimized-parameters well represented the various joint tissues, which were included in the model, suggested by their similarity with the respective estimated-parameters, also supporting hypothesis 2. Indeed, the estimated and optimized centres of the aforementioned spheres' were not significantly different. Furthermore, the optimized-spheres-residuals, although significantly higher than the measured-residuals, were small (≤ 0.9 mm), indicating that all spheres well fitted the bone-cartilages' surfaces. Finally, the TFJ optimized-parameters' largest and average RMSDs (12.2 mm and 0.3 mm) were similar to Ottoboni et al. (2010) TFJ mechanisms (11.2 mm and 2.4 mm).

Hypotheses 3 and 4 were only partially upheld. Similar to Beynnon et al. (1996) we found small variations in the TFJ and PFJ translations' ROMs, probably due to the small variations in most of the TFJ and PFJ optimized-parameters. However, the TFJ medial tibial spheres exhibited large variation, which did not affect the TFJ kinematics, except maybe the AA rotation which showed large

Table 5
The TCJ models' locations of spheres' centres, ligaments' attachments, links' lengths and spheres' radii (average ± std), estimated from the MRI and adjusted by optimization.

Direction	Estimated/ optimized	Location in the distal tibia and distal fibula (mm)									
		CaFi (${}^{TIB}F_1$)	RMSD	TiCa (${}^{TIB}F_2$)	RMSD	Distal-medial fibula (${}^{TIB}F_3$)	RMSD	Medial tibial mortise (${}^{TIB}F_4$)	RMSD	Lateral tibial mortise (${}^{TIB}F_5$)	RMSD
X	Estimated	3.32 ± 2.03	1.39 ± 0.92	-6.83 ± 3.23	2.34 ± 1.44	-83.40 ± 253.76	2.35 ± 1.60	−0.71 ± 0.85	1.85 ± 1.20	3.01 ± 0.82	2.13 ± 1.33
	Optim2	3.28 ± 2.59		−7.59 ± 4.81		−83.94 ± 254.04		−1.33 ± 2.28		1.98 ± 2.61	
Y	Estimated	−5.40 ± 2.01	0.99 ± 0.69	11.33 ± 1.97	0.63 ± 0.51	−4.77 ± 52.32	2.15 ± 1.35	−6.27 ± 3.07	2.06 ± 1.54	−4.33 ± 1.97	1.68 ± 1.09
	Optim2	−5.55 ± 1.94		11.36 ± 2.48		−6.08 ± 51.43		−5.88 ± 3.57		−4.65 ± 3.11	
Z	Estimated	25.14 ± 2.89	1.38 ± 1.05	−27.78 ± 3.59	1.38 ± 1.12	−201.67 ± 582.17	2.32 ± 1.66	−13.62 ± 2.10	3.10 ± 1.66	4.30 ± 1.54	1.87 ± 1.39
	Optim2	24.87 ± 3.11		-27.68 ± 4.35		-202.18 ± 581.50		-12.09 ± 3.00		5.28 ± 2.64	
		Location in the calcaneus and talus (mm)									
		CaFi(${}^{TAL}E_1$)	RMSD	TiCa (${}^{TAL}E_2$)	RMSD	Lateraltalus (${}^{TAL}E_3$)	RMSD	Medial trochlea tali (${}^{TAL}E_4$)	RMSD	Lateral trochlea tali (${}^{TAL}E_5$)	RMSD
X	Estimated	−20.65 ± 7.93	2.39 ± 2.95	§−6.91 ± 1.97	1.89 ± 0.96	−23.20 ± 78.09	2.06 ± 1.43	−0.16 ± 0.61	1.43 ± 0.71	−0.14 ± 0.76	1.36 ± 0.68
	Optim2	−21.62 ± 10.30		−8.47 ± 2.91		−23.52 ± 78.37		0.36 ± 1.18		0.29 ± 1.34	
Y	Estimated	−28.61 ± 3.27	2.92 ± 2.27	−21.72 ± 3.17	0.62 ± 0.48	−4.05 ± 23.69	3.09 ± 1.39	−14.07 ± 3.52	2.12 ± 1.39	−11.69 ± 2.54	2.29 ± 1.46
	Optim2	−28.66 ± 4.20		−22.04 ± 2.98		−3.18 ± 23.20		−14.42 ± 4.24		−12.33 ± 3.82	
Z	Estimated	24.56 ± 4.08	0.70 ± 0.49	§−14.94 ± 3.10	1.08 ± 0.76	−45.88 ± 267.73	1.99 ± 1.55	-6.14 ± 1.56	2.63 ± 1.38	11.09 ± 1.91	2.28 ± 1.34
	Optim2	24.56 ± 4.20		−13.95 ± 2.93		−45.74 ± 266.69		−7.70 ± 3.49		11.38 ± 3.56	
		Links lengths (mm)									
		CaFi(${}^{TCJ}L_1$)	RMSD	TiCa(${}^{TCJ}L_2$)	RMSD	Fibula-talus(${}^{TCJ}L_3$)	RMSD	Medial tibia-talus (${}^{TCJ}L_4$)	RMSD	Lateral tibia-talus (${}^{TCJ}L_5$)	RMSD
Length	Estimated	26.18 ± 2.83	3.28 ± 2.71	§24.43 ± 3.01	1.39 ± 1.28	169.49 ± 388.99	3.19 ± 2.46	§2.60 ± 1.67	4.77 ± 2.09	§1.51 ± 0.84	3.93 ± 2.06
	Optim2	26.99 ± 6.00		25.81 ± 3.37		171.41 ± 388.92		7.37 ± 2.03		5.40 ± 2.16	

		Radii of the distal tibia, distal fibula and talus spheres (mm)											
		Distal-medial Fibula (${}^{FIB}r_1$)	RMSD	Medial tibial mortise (${}^{TIB}r_3$)	RMSD	Lateral tibial mortise (${}^{TIB}r_4$)	RMSD	Lateral talus (${}^{TAL}r_1$)	RMSD	Medial trochlea tali (${}^{TAL}r_2$)	RMSD	Lateral trochlea tali (${}^{TAL}r_3$)	RMSD
Radii	Estimated	255.75 ± 626.95	2.46	26.43 ± 3.79	1.95	23.98 ± 2.16	1.69	124.32 ± 257.92	1.92	24.30 ± 3.47	1.95	23.17 ± 2.70	1.99 ± 1.38
	Optim2	256.29 ± 626.44	± 1.63	26.08 ± 3.53	± 1.61	24.60 ± 2.97	± 1.13	124.44 ± 256.82	± 1.29	24.90 ± 4.01	± 1.23	23.98 ± 3.21	

§ Difference (with paired *t*-tests) between estimated and optimized (from Optim2) values ($p < 0.03$).

Table 6
Sensitivity analysis showing the coefficients (average ± std) of the 2nd order polynomial fitted to the objective function values (G_2).

TFJ ligament attachment points			
	X	Y	Z
ACL in tibia ($^{TIB}A_1$)	0.03 ± 0.05	0.01 ± 0.01	0.02 ± 0.03
PCL in tibia ($^{TIB}A_2$)	0.00 ± 0.01	0.00 ± 0.00	0.01 ± 0.01
MCL in tibia ($^{TIB}A_3$)	0.01 ± 0.02	0.00 ± 0.00	0.00 ± 0.00
ACL in femur ($^{FEM}B_1$)	0.09 ± 0.15	0.03 ± 0.03	0.01 ± 0.03
PCL in femur ($^{FEM}B_2$)	0.19 ± 0.36	0.33 ± 0.38	0.06 ± 0.08
MCL in femur ($^{FEM}B_3$)	0.74 ± 1.20	0.12 ± 0.15	0.03 ± 0.09
TFJ tibial plateau spheres centres			
Medial ($^{TIB}A_4$)	0.00 ± 0.00	0.00 ± 0.00	0.01 ± 0.01
Lateral ($^{TIB}A_5$)	0.02 ± 0.03	0.00 ± 0.00	0.00 ± 0.00
PFJ PT attachment points			
PT in tibia (^{TIB}C)	0.01 ± 0.04	0.00 ± 0.00	0.00 ± 0.00
PT in patella (^{PAT}D)	0.01 ± 0.03	0.01 ± 0.03	0.00 ± 0.01
PFJ femoral patellar spheres centres			
Medial ($^{FEM}p_1$)	0.33 ± 0.37	0.24 ± 0.25	0.02 ± 0.06
Lateral ($^{FEM}p_2$)	0.27 ± 0.38	0.24 ± 0.27	0.02 ± 0.06
TCJ ligament attachment points			
CaFi in fibula ($^{TIB}F_1$)	0.03 ± 0.05	0.02 ± 0.05	0.01 ± 0.02
TiCa in tibia ($^{TIB}F_2$)	0.07 ± 0.18	0.05 ± 0.20	0.09 ± 0.33
CaFi in calcaneus ($^{TAL}E_1$)	0.00 ± 0.00	0.00 ± 0.01	0.00 ± 0.00
TiCa in calcaneus ($^{TAL}E_2$)	0.03 ± 0.06	0.01 ± 0.03	0.01 ± 0.02
TCJ spheres centres			
Distal-medial fibula ($^{TIB}F_3$)	0.14 ± 0.36	0.08 ± 0.20	0.04 ± 0.11
Medial tibial mortise ($^{TIB}F_4$)	0.68 ± 1.06	0.42 ± 0.87	0.25 ± 0.53
Lateral tibial mortise ($^{TIB}F_5$)	0.65 ± 0.93	0.73 ± 1.36	0.22 ± 0.40
Lateral talus ($^{TAL}E_3$)	0.20 ± 0.71	0.02 ± 0.05	0.04 ± 0.10
Medial trochlea tali ($^{TAL}E_4$)	0.66 ± 1.09	0.35 ± 0.88	0.34 ± 0.60
Lateral trochlea tali ($^{TAL}E_5$)	0.31 ± 0.50	0.33 ± 1.01	0.17 ± 0.40

means and ROMs' variations. Similarly, most TCJ optimized-parameters exhibited small variations except the lateral talo-fibular spheres' centres; likewise they do not seem to affect the TCJ means and ROMs' variations. Interestingly, the TCJ had "non-sagittal plane" IE and AA rotations that approximated a universal joint (Sancisi et al., 2014) rather than a pure hinge joint (Isman and Inman, 1968; Kapandji, 1987), which is commonly used in generic models (Hamner et al., 2010).

Some participants' tibial spheres' centres' had large radii suggesting that their tibial surfaces were nearly flat. This has been reported in other populations (Hashemi et al., 2008; Matsuda et al., 1999), and other's opted to fit planes to these surfaces in their TFJ mechanisms (Parenti-Castelli and Di Gregorio, 2000). However, the use of spheres allow a better approximation of measured kinematics (Ottoboni et al., 2010) and is recommended.

The two participants' results also suggested that joint kinematics were influenced by joint geometries, supporting Hypothesis 5. These participants had very different fitted spheres' centres due to different tibial surfaces' geometries. Subsequently, their TFJ kinematics metrics were different, although their translations' patterns were similar. Participant 2 had a deeper medial tibial concavity which constrained the TFJ PD translation, resulting in a smaller PD ROM (Hashemi et al., 2008) and a smaller AA ROM. Furthermore, participant 2's less concave lateral surface allowed a larger AP translation (Johal et al., 2005). Since these parameters are not accounted for in generic models, subject-specific models may potentially estimate more accurate personalized kinematics, although this will need to be assessed in future studies. This is very important since joint kinematics highly influence joint loading (Gerus et al., 2013; Li et al., 2004; Zheng et al., 2014). However, a full examination of the effects of participant variability on estimated kinematics was beyond the scope of this paper, due to the limited number of participants, which would require a much larger population exhibiting geometrical variability, since a minimum of 16 parameters were optimized for each model.

The models were sensitive to the PFJ and TCJ sphere centres, revealed by high quadratic coefficients. Therefore, these parameters need to be properly estimated and optimized. In contrast, the PT ligaments' attachments points had very small coefficients and thus optimizing these parameters might not be necessary. Similar results were showed by: (i) El Habachi et al. (2015); equivalent TFJ, PFJ and TCJ mechanisms showed high sensitivity to the PFJ hinge axis and less sensitive to the PT attachments' points and (ii) Sancisi and Parenti-Castelli, (2011); accuracy of PFJ model was most influenced by the position of PFJ spheres' centres.

The proposed models and study have limitations. We were unable to validate each participant's estimated kinematics using measured kinematics, due to time and budget constraints. However, the mechanism-based models have been previously well validated using subject-specific cadaveric data (Franci et al., 2009; Sancisi and Parenti-Castelli, 2011). Furthermore, Clément et al. (2015) recently implemented a similar personalized TFJ mechanism model, with a mix of subject-specific and generic parameters, which accurately estimated the TFJ kinematics of a squat measured using biplanar radiography. Finally, we expect our participants' measured kinematics curves' patterns to be similar to the published kinematics. In fact, the PFJ kinematics included not just *in vitro* but also *in vivo* kinematics, which generally presented similar curves' patterns, with high correlations, except for the AA, IE and ML potentially because of their small ROMs (see App. C). We only created models for 14 participants, and although not a large population, it is considerably more than other studies which developed MRI personalized model-derived kinematics (Bei and Fregly, 2004; Kainz et al., 2016; Sandholm et al., 2011; Scheys et al., 2008; Sreenivasa et al., 2016; Valente et al., 2015). Optimization required ~10 h computation time, similar to that reported previously (Ottoboni et al., 2010). However, optimization of only the crucial parameters identified in the sensitivity analysis, and code parallelization may reduce computation times. Finally, the proposed models were for published passive motion, possibly limiting applicability to loaded motion. However, passive kinematics may provide good estimates of *in vivo* joint motion (Sancisi and Parenti-Castelli, 2011), considering the reported similarities between unloaded and physiologically loaded joints (Lu et al., 2008; Myers et al., 2012). Furthermore, adding a lateral collateral ligament to the current TFJ mechanism and using minimally deformable ligaments, Gasparutto et al. (2015) attained accurate tracking of *in vivo* TFJ kinematics during running. However, they only used average cadaveric parameters, and including MRI-derived subject-specific parameters may further improve estimation of *in vivo* motion.

Summarizing, a robust new optimization method to estimate subject-specific TFJ, PFJ and TCJ joint kinematics was presented, with the models' parameters estimated off the individuals' MRIs. Parameter optimization did not require individually measured kinematics, but relied on transformed published kinematics that we created from literature (supplementary materials). The models' optimized-parameters well represented the participants' anatomical tissues, and the estimated kinematics had curve patterns similar to the published kinematics. Future work should focus on comparing the mechanisms' kinematics with those from generic models scaled for the same participants (Walker et al., 1988; Yamaguchi and Zajac, 1989), and assemble their mechanisms into complete OpenSim subject-specific lower-limb models to enable

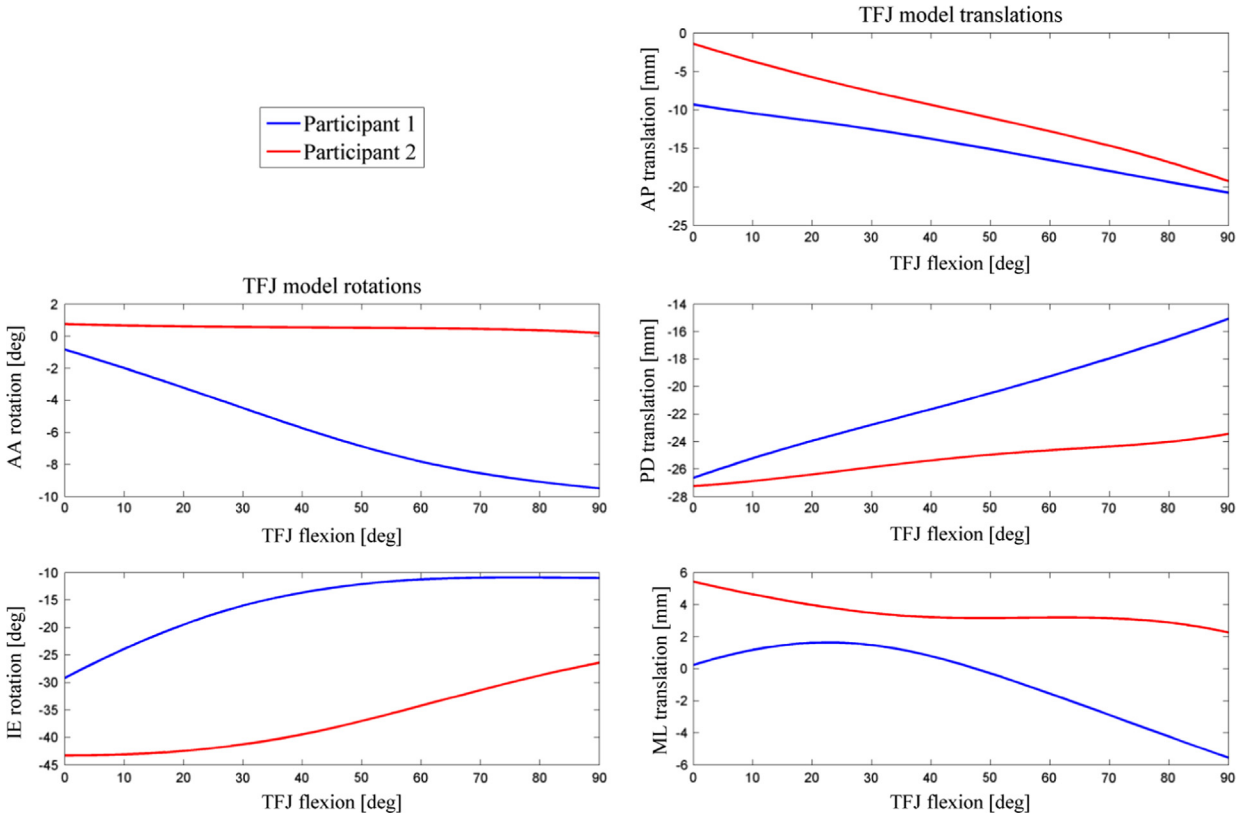

Fig. 4. Comparison between subject-specific TFJ model kinematics from two participants with different medial tibial plateau. Participants' 1 had a medial tibial plateau sphere centre (${}^{TIB}A_4$) and radius (${}^{TIB}r_1$) of (−754.5, 3051.2, −515.78) mm and 3186.8 mm respectively, while participants' 2 measures were (−19.9, 126.2, −18.2) mm and 131.7 mm. Participants' 1 had a lateral tibial plateau sphere centre (${}^{TIB}A_5$) and radius of (${}^{TIB}r_2$) of (15.8, −51.2, −2.7) mm and 54.1 mm respectively, while participants' 2 measures were (34.1, −282.2, −57.0) mm and 291.5 mm. AP ROM was 12mm for participant 1 and 18 mm for participant 2, PD ROM was 12 mm for participant 1 and 4 mm for participant 2 while AA ROM was 9° for participant 1 and 1° for participant 2. All correlations coefficients were $\rho \geq 0.7$ with $p \leq 0.05$. These TFJ kinematic differences are probably due to the medial and lateral tibial plateau sizes. (For interpretation of the references to colour in this figure legend, the reader is referred to the web version of this article.)

inverse kinematics and dynamics estimates of joint angles and moments during motion.

Conflict of interest statement

All authors declare that there is no conflict of interest and no financial or personal relationships with other people or organizations that could inappropriately influence (bias) their work.

Appendix A. Supplementary material

Supplementary data associated with this article can be found in the online version at http://dx.doi.org/10.1016/j.jbiomech.2016.12.018.

References

Anglin, C., Ho, K.C.T., Briard, J.-L., de Lambilly, C., Plaskos, C., Nodwell, E., Stindel, E., 2008. In vivo patellar kinematics during total knee arthroplasty. Comput. Aided Surg. 13, 377–391.
Arnold, E., Ward, S., Lieber, R.L., Delp, S., 2010. A model of the lower limb for analysis of human movement. Ann. Biomed. Eng. 38, 269–279.
Bei, Y., Fregly, B.J., 2004. Multibody dynamic simulation of knee contact mechanics. Med. Eng. Amp. Phys. 26, 777–789.
Belvedere, C., Catani, F., Ensini, A., Moctezuma de la Barrera, J.L., Leardini, A., 2007. Patellar tracking during total knee arthroplasty: an in vitro feasibility study. Knee Surg. Sport. Traumatol. Arthr 15, 985–993.
Benjamini, Y., Hochberg, Y., 1995. Controlling the false discovery rate: a practical and powerful approach to multiple testing. J. R. Stat. Soc. Ser. B (Methodol.) 57, 289–300.
Beynnon, B., Yu, J., Huston, D., Fleming, B., Johnson, R., Haugh, L., Pope, M.H., 1996. A sagittal plane model of the knee and cruciate ligaments with application of a sensitivity analysis. J. Biomech. Eng. 118, 227–239.
Clément, J., Dumas, R., Hagemeister, N., de Guise, J.A., 2015. Soft tissue artifact compensation in knee kinematics by multi-body optimization: performance of subject-specific knee joint models. J. Biomech. 48, 3796–3802.
Damsgaard, M., Rasmussen, J., Christensen, S.T., Surma, E., de Zee, M., 2006. Analysis of musculoskeletal systems in the AnyBody Modeling System. Simul. Model. Pract. Theory 14, 1100–1111.
Della Croce, U., Cappozzo, A., Kerrigan, D.C., 1999. Pelvis and lower limb anatomical landmark calibration precision and its propagation to bone geometry and joint angles. Med. Biol. Eng. Comput. 37, 155–161.
Delp, S.L., Loan, J.P., Hoy, M.G., Zajac, F.E., Topp, E.L., Rosen, J.M., 1990. An interactive graphics-based model of the lower extremity to study orthopaedic surgical procedures. Biomed. Eng. IEEE Trans. 37, 757–767.
Delp, S.L., Anderson, F.C., Arnold, A.S., Loan, P., Habib, A., John, C.T., Guendelman, E., Thelen, D.G., 2007. OpenSim: open-source software to create and analyze dynamic simulations of movement. Biomed. Eng., IEEE Trans. 54, 1940–1950.
Duprey, S., Cheze, L., Dumas, R., 2010. Influence of joint constraints on lower limb kinematics estimation from skin markers using global optimization. J Biomech. 43, 2858–2862.
El Habachi, A., Moissenet, F., Duprey, S., Cheze, L., Dumas, R., 2015. Global sensitivity analysis of the joint kinematics during gait to the parameters of a lower limb multi-body model. Med. Biol. Eng. Comput. 53, 655–667.
Franci, R., Parenti-Castelli, V., Belvedere, C., Leardini, A., 2009. A new one-DOF fully parallel mechanism for modelling passive motion at the human tibiotalar joint. J. Biomech. 42, 1403–1408.
Fuss, F.K., 1989. Anatomy of the cruciate ligaments and their function in extension and flexion of the human knee joint. Am. J. Anat. 184, 165–176.
Gasparutto, X., Sancisi, N., Jacquelin, E., Parenti-Castelli, V., Dumas, R., 2015. Validation of a multi-body optimization with knee kinematic models including ligament constraints. J. Biomech. 48, 1141–1146.

Gerus, P., Sartori, M., Besier, T.F., Fregly, B.J., Delp, S.L., Banks, S.A., Pandy, M.G., D'Lima, D.D., Lloyd, D.G., 2013. Subject-specific knee joint geometry improves predictions of medial tibiofemoral contact forces. J. Biomech. 46, 2778–2786.
Grood, E.S., Suntay, W.J., 1983. A joint coordinate system for the clinical description of three-dimensional motions: application to the knee. J. Biomech. Eng. 105, 136–144.
Hamner, S.R., Seth, A., Delp, S.L., 2010. Muscle contributions to propulsion and support during running. J. Biomech. 43, 2709–2716.
Hashemi, J., Chandrashekar, N., Gill, B., Beynnon, B.D., Slauterbeck, J.R., Schutt Jr., R. C., Mansouri, H., Dabezies, E., 2008. The geometry of the tibial plateau and its influence on the biomechanics of the tibiofemoral joint. J Bone Jt. Surg. Am. 90, 2724–2734.
Hicks, J.L., Uchida, T.K., Seth, A., Rajagopal, A., Delp, S.L., 2015. Is my model good enough? Best practices for verification and validation of musculoskeletal models and simulations of movement. J Biomech. Eng. 137, 26.
Isman, R., Inman, V., 1968. Anthropometric studies of the human foot and ankle. Biomechanics Laboratory. University of California, San Francisco, Berkeley, p. 58 (The Laboratory, San Francisco).
Johal, P., Williams, A., Wragg, P., Hunt, D., Gedroyc, W., 2005. Tibio-femoral movement in the living knee. A study of weight bearing and non-weight bearing knee kinematics using 'interventional' MRI. J. Biomech. 38, 269–276.
Kainz, H., Modenese, L., Lloyd, D., Maine, S., Walsh, H., Carty, C., 2016. Joint kinematic calculation based on clinical direct kinematic versus inverse kinematic gait models. J. Biomech. 49, 1658–1669.
Kapandji, I.A., 1987. The Physiology of the Joints, 5 ed. Churchill Livingstone, London.
Leardini, A., O'Connor, J.J., Catani, F., Giannini, S., 1999. A geometric model of the human ankle joint. J. Biomech. 32, 585–591.
Lerner, Z.F., DeMers, M.S., Delp, S.L., Browning, R.C., 2015. How tibiofemoral alignment and contact locations affect predictions of medial and lateral tibiofemoral contact forces. J. Biomech. 48, 644–650.
Li, G., DeFrate, L.E., Zayontz, S., Park, S.E., Gill, T.J., 2004. The effect of tibiofemoral joint kinematics on patellofemoral contact pressures under simulated muscle loads. J. Orthop. Res. 22, 801–806.
Lu, T.-W., Tsai, T.-Y., Kuo, M.-Y., Hsu, H.-C., Chen, H.-L., 2008. In vivo three-dimensional kinematics of the normal knee during active extension under unloaded and loaded conditions using single-plane fluoroscopy. Med. Eng. Phys. 30, 1004–1012.
Matsuda, S., Miura, H., Nagamine, R., Urabe, K., Ikenoue, T., Okazaki, K., Iwamoto, Y., 1999. Posterior tibial slope in the normal and varus knee. Am. J Knee Surg. 12, 165–168.
Modenese, L., Phillips, A.T.M., Bull, A.M.J., 2011. An open source lower limb model: hip joint validation. J. Biomech. 44, 2185–2193.
Myers, C.A., Torry, M.R., Shelburne, K.B., Giphart, J.E., LaPrade, R.F., Woo, S.L.-Y., Steadman, J.R., 2012. In vivo tibiofemoral kinematics during 4 functional tasks of increasing demand using biplane fluoroscopy. Am. J. Sport. Med. 40, 170–178.
Ottoboni, A., Parenti-Castelli, V., Sancisi, N., Belvedere, C., Leardini, A., 2010. Articular surface approximation in equivalent spatial parallel mechanism models of the human knee joint: an experiment-based assessment. Proc. Inst. Mech. Eng., Part H: J. Eng. Med. 224, 1121–1132.
Parenti-Castelli, V., Di Gregorio, R., 2000. Academic, K. (Ed.), Parallel Mechanisms Applied to the Human Knee Passive Motion Simulation. Advances in Robot Kinematics, pp. 333–344.
Rovick, J.S., Reuben, J.D., Schrager, R.J., Walker, P.S., 1991. Relation between knee motion and ligament length patterns. Clin. Biomech. 6, 213–220.
Sancisi, N., Parenti-Castelli, V., 2011. A new kinematic model of the passive motion of the knee inclusive of the patella. J. Mech. Robot. 3 (041003-041003).
Sancisi, N., Zannoli, D., Parenti-Castelli, V., Belvedere, C., Leardini, A., 2011. A one-degree-of-freedom spherical mechanism for human knee joint modelling. Proc. Inst. Mech. Eng., Part H: J. Eng. Med. 225, 725–735.
Sancisi, N., Baldisserri, B., Parenti-Castelli, V., Belvedere, C., Leardini, A., 2014. One-degree-of-freedom spherical model for the passive motion of the human ankle joint. Med. Biol. Eng. Comput. 52, 363–373.
Sandholm, A., Schwartz, C., Pronost, N., de Zee, M., Voigt, M., Thalmann, D., 2011. Evaluation of a geometry-based knee joint compared to a planar knee joint. Vis. Comput. 27, 161–171.
Scheys, L., Van Campenhout, A., Spaepen, A., Suetens, P., Jonkers, I., 2008. Personalized MR-based musculoskeletal models compared to rescaled generic models in the presence of increased femoral anteversion: effect on hip moment arm lengths. Gait Amp. Posture 28, 358–365.
Scheys, L., Desloovere, K., Suetens, P., Jonkers, I., 2011. Level of subject-specific detail in musculoskeletal models affects hip moment arm length calculation during gait in pediatric subjects with increased femoral anteversion. J. Biomech. 44, 1346–1353.
Sreenivasa, M., Chamorro, C.J.G., Gonzalez-Alvarado, D., Rettig, O., Wolf, S.I., 2016. Patient-specific bone geometry and segment inertia from MRI images for model-based analysis of pathological gait. J. Biomech. 49, 1918–1925.
Tsai, L.C., Colletti, P.M., Powers, C.M., 2012. Magnetic resonance imaging-measured muscle parameters improved knee moment prediction of an EMG-driven model. Med. Sci. Sport. Exerc. 44, 305–312.
Valente, G., Pitto, L., Stagni, R., Taddei, F., 2015. Effect of lower-limb joint models on subject-specific musculoskeletal models and simulations of daily motor activities. J. Biomech. 48, 4198–4205.
Walker, P.S., Rovick, J.S., Robertson, D.D., 1988. The effects of knee brace hinge design and placement on joint mechanics. J. Biomech. 21, 965–974.
Wilson, D.R., Feikes, J.D., O'Connor, J.J., 1998. Ligaments and articular contact guide passive knee flexion. J. Biomech. 31, 1127–1136.
Wu, G., Siegler, S., Allard, P., Kirtley, C., Leardini, A., Rosenbaum, D., Whittle, M., D'Lima, D.D., Cristofolini, L., Witte, H., Schmid, O., Stokes, I., 2002. ISB recommendation on definitions of joint coordinate system of various joints for the reporting of human joint motion—part I: ankle, hip, and spine. J. Biomech. 35, 543–548.
Yamaguchi, G.T., Zajac, F.E., 1989. A planar model of the knee joint to characterize the knee extensor mechanism. J. Biomech. 22, 1–10.
Zheng, L., Li, K., Shetye, S., Zhang, X., 2014. Integrating dynamic stereo-radiography and surface-based motion data for subject-specific musculoskeletal dynamic modeling. J. Biomech. 47, 3217–3221.